

A postgraduate laboratory experiment to set up a single-photon detector using MKIDs

**Pietro Campana, Rodolfo Carobene, Eleonora Cipelli,
Marco Gobbo, Aurora Perego, Davide Vertemati ‡**

Dipartimento di Fisica, Università degli Studi di Milano-Bicocca, I-20126 Milano,
Italy

E-mail: p.campana1@campus.unimib.it

E-mail: r.carobene@campus.unimib.it

E-mail: e.cipelli@campus.unimib.it

E-mail: m.gobbo4@campus.unimib.it

E-mail: a.perego39@campus.unimib.it

E-mail: d.vertemati@campus.unimib.it

Abstract.

This paper presents a laboratory activity aimed at developing knowledge and expertise in microwave applications at cryogenic temperatures. The experience focuses on the detection of single infrared photons through Microwave Kinetic Inductance Detectors (MKIDs). The experimental setup, theoretical concepts, and activities involved are detailed, highlighting the skills and knowledge gained through the experience. This experiment is designed for postgraduate students in the field of quantum technologies.

1. Introduction

Over the past two decades, there has been a significant increase in research and development of new detectors that operate at cryogenic temperatures leveraging the phenomenon of superconductivity [3, 17]. While detectors based on semiconductors have already achieved high performances [8], the smaller band gap of superconductors offers the potential for higher sensitivities and better energy resolutions. Recent and promising devices of this kind are Microwave Kinetic Inductance Detectors (MKIDs) [21], first proposed in 2003 by researchers from the California Institute of Technology and the Jet Propulsion Laboratory [4]. An MKID consists of a superconducting resonator whose resonant frequency changes in response to the absorption of photons. In addition to their high sensitivity when used as photon detectors, MKIDs can be arranged in multiplexed arrays. This allows for the readout of multiple detectors using a single

‡ All authors have contributed equally to this paper.

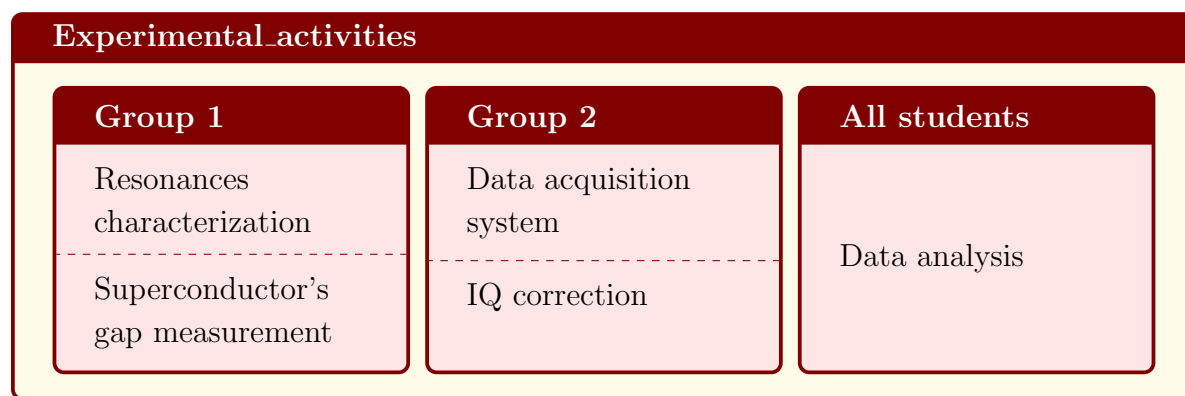
A postgraduate laboratory experiment to set up a single-photon detector using MKIDs²

electrical connection carrying signals at different frequencies, implementing a technique known as microwave multiplexing. In a cryogenic experiment, multiplexing can be used to simplify the experimental setup inside the cryostat, reducing the heat carried by electrical connections.

Postgraduate laboratory experiences provide students with an opportunity to develop their experimental skills and apply their theoretical knowledge, serving as a hands-on introduction to current research and technologies. Working on a complex cryogenic project from start to finish also offers direct experience in the operation of many important instruments tied to multiple disciplines, from electronics to quantum mechanics, while facing the various practical problems that will inevitably arise. This paper presents the experimental activities carried out by six students at the Cryogenics Laboratory of Università degli Studi di Milano-Bicocca. Leveraging the resources of a previous work [16], a single photon detector employing MKIDs was set up and characterized over the course of two semesters.

As shown in box 1, the experiment was organized into different activities that could be carried out separately. The students were divided into two groups, with the first one focusing on the characterization of the MKID's resonances and superconductor band gap, while the second group worked on the data acquisition system and the calibration of the raw data acquired with the custom circuit used in photon detection. Finally, data analysis carried out by both groups together confirmed the detection of a small number of photons.

In section 2 the theory necessary to perform the experiment is presented, while section 3 describes the experimental setup. Finally, section 4 details all the activities and the achieved results.



Box 1: Outline of the experimental activities.

2. Theoretical background

The superconducting properties of a material arise from the formation of Cooper pairs due to interactions between electrons and phonons. The energy required to break a

Cooper pair is 2Δ , where Δ is the superconductor's energy gap, which is related to the critical temperature T_c [2, 15]:

$$2\Delta \approx 3.5k_B T_c \quad (1)$$

When Cooper pairs are broken, the resulting electrons are called quasiparticles. In a metal, the mobility of quasiparticles is limited by their short scattering distance. On the other hand, Cooper pairs can move freely and possess an inertia that causes a delay in their response to a changing field, giving rise to a kinetic inductance term L_k in addition to the conventional magnetic inductance L_m .

Kinetic inductance can be exploited to build cryogenics detectors. In particular, Microwave Kinetic Inductance Detectors (MKIDs) are LC resonators whose resonant frequency is sensitive to the interaction with photons. When a photon with energy greater than 2Δ is absorbed by the resonator, it breaks Cooper pairs into quasiparticles, leading to an increase in the kinetic inductance which alters the resonant frequency of the MKID. To measure their response, MKIDs are usually capacitively coupled to a transmission line.

To study the response of MKIDs, we must first consider them as components in a RF network. An RF network can be described in terms of the relations between the incident and reflected waves at each of its ports, which can be organized in a complex-valued matrix known as the S-matrix. The response of a device can be expressed through the forward gain parameter $S_{21} = \frac{V_2^-}{V_1^+}$, where V_2^- is the wave transmitted across it and V_1^+ is the incident one.

For an ideal capacitively coupled resonator of resonant frequency f_0 , S_{21} is given by [20]:

$$S_{21}(f) = 1 - \frac{Q}{Q_c} \frac{1}{1 + 2jQ \frac{f-f_0}{f_0}} \quad (2)$$

where Q is the resonance's total quality factor, which represents the energy storage efficiency of the resonator, determining the sensitivity of the device. It is defined as the ratio of the stored energy to the energy dissipated per cycle, or equivalently as the ratio of the resonant frequency to the resonance's bandwidth. The quality factor has two contributions:

$$\frac{1}{Q} = \frac{1}{Q_i} + \frac{1}{Q_c} \quad (3)$$

where Q_c accounts for the capacitive coupling to the feedline, while Q_i accounts for all other losses intrinsic to the resonator, including the resistive contribution due to quasiparticles and the presence of two-level systems on the material's surface [18].

Measuring the internal quality factor of an MKID at different temperatures allows us to find its T_c from eq. (1) by indirectly measuring Δ . Given Δ_0 the energy gap at $T = 0$ K, at low frequencies $\hbar\omega \ll \Delta_0$ and low temperatures $k_B T \ll \Delta_0$, the complex conductivity $\sigma = \sigma_1 + j\sigma_2$ of a superconductor can be approximated by analytical formulas:

$$\frac{\sigma_1(\omega)}{\sigma_n} \approx \frac{4\Delta}{\hbar\omega} e^{-\frac{\Delta_0}{k_B T}} \sinh(\xi) K_0(\xi), \quad \xi = \frac{\hbar\omega}{2k_B T}, \quad (4)$$

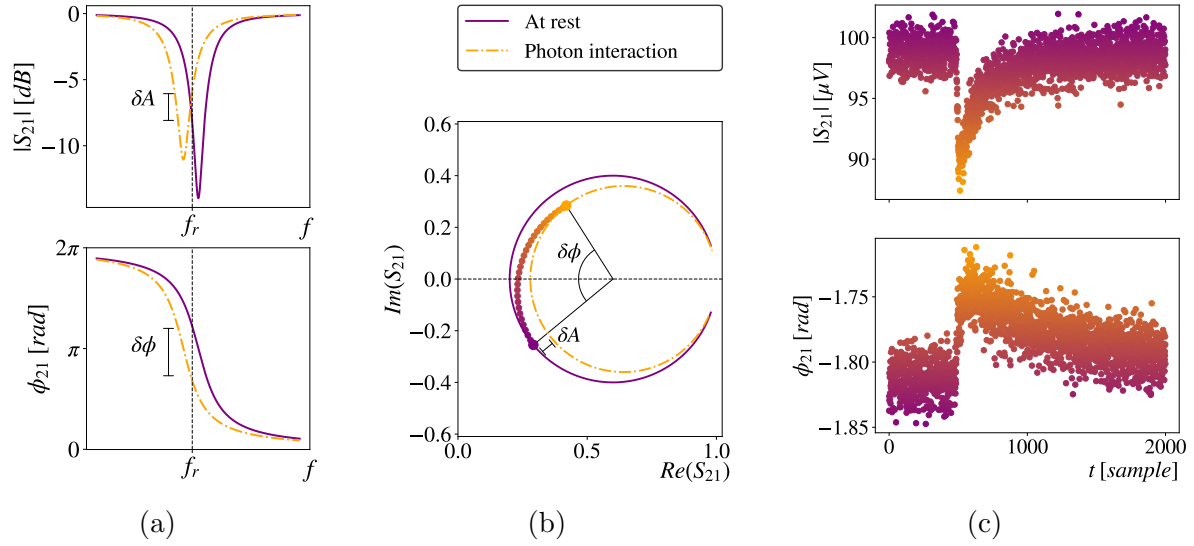


Figure 1: Working principle of an MKID. (a) The resonance profile in the frequency domain (purple line). The interaction with a photon alters its frequency and shape (dashed orange line). If the MKID is probed at a fixed frequency f_r , a shift both in amplitude δA and in phase $\delta\phi$ can be observed. (b) In the complex plane, the shift appears as moving from a point on the outer (purple) circle to a point on the smaller one (dashed orange line), tracing the path followed by the plotted dots. (c) Example of a raw signal's amplitude and phase in the time domain.

$$\frac{\sigma_2(\omega)}{\sigma_n} \approx \frac{\pi\Delta}{\hbar\omega} \left[1 - 2e^{-\frac{\Delta_0}{k_B T}} e^{-\xi} I_0(-\xi) \right] \quad (5)$$

where I_0 and K_0 are the modified Bessel functions of the first and second kind, while σ_n is the normal (non-superconductive) conductivity of the metal. The complex conductivity determines the temperature dependence of the internal quality factor:

$$\frac{1}{Q_i(T)} = \frac{1}{Q_i(0)} + \frac{\alpha\sigma_1(T, \Delta)}{2\sigma_2(T, \Delta)}, \quad \alpha = \frac{L_k}{L_k + L_m} \quad (6)$$

Therefore, the energy gap can be estimated by substituting σ_1 and σ_2 with their approximate expressions (eqs. (4) and (5)) and fitting a set of Q_i values measured at different temperatures in the appropriate range. On the other hand, the kinetic inductance fraction α can be computed with simulations.

Figure 1 illustrates how the energy deposited by a photon interacting with an MKID can be measured [6]. To detect the shift of the resonance, the MKID is probed at a fixed frequency while measuring the phase and amplitude of S_{21} . In the complex plane, where resonances correspond to circles, an event traces a trajectory between a point on an outer circle and a point on a smaller one. The resulting observed amplitude shift δA is proportional to the energy deposited in the resonator. However, the phase excursion $\delta\phi$ typically generates a much larger and more identifiable signal than the amplitude, even if it presents excess noise due to the influence of the two-level systems acting only tangentially to the circles. Since an estimator proportional to the energy can also be

A postgraduate laboratory experiment to set up a single-photon detector using MKIDs5

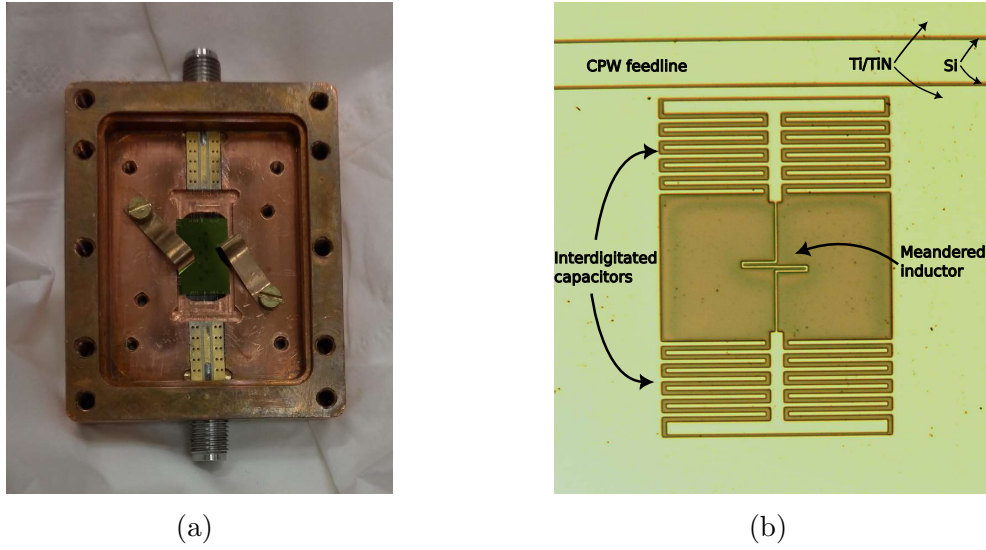


Figure 2: (a) The MKIDs chip in the copper holder needed to screw it to the mixing chamber plate. It contains eight resonators placed in a grid. (b) Zoom-in view of a single resonator.

easily obtained from $\delta\phi$, the readout of MKIDs often relies on the measurement of the phase of S_{21} .

Moreover, the increased number of quasiparticles generated in the interaction dissipates more energy, reducing the internal quality factor. In addition to the shift of the resonant frequency, this also results in a slight change in the shape of its profile.

3. Experimental setup

The detector consists of a custom chip containing 8 MKIDs with different resonant frequencies. The resonators (see fig. 2) were fabricated using interdigitated capacitors [12] and are coupled to a shared Coplanar Waveguide (CPW). The chip, manufactured by Fondazione Bruno Kessler (FBK), is made of a silicon substrate on which alternating layers of titanium and titanium nitride (TiN) [14] are deposited. Since MKIDs are superconducting detectors, they operate at temperatures significantly below the critical point of TiN. To achieve this, the chip is placed inside a copper holder and attached to the mixing chamber plate of a dilution cryostat manufactured by Oxford Instruments, which is capable of reaching a minimum temperature of ~ 30 mK.

An LSP-1550-FC laser diode by Thorlabs was used to generate photons with an energy of 0.8 eV. An intermittent power supply was provided via direct connection to a function generator, in order to generate a small amount of photons. To check the correct functioning of the device, the output of the laser was visualized with an oscilloscope, using a circuit made of a photodiode, an amplifier, and an RC filter as shown in fig. 3.

To establish a connection between the diode, operating at room temperature, and the MKIDs located within the cryostat, an optical fiber with a -20 dB attenuator was

A postgraduate laboratory experiment to set up a single-photon detector using MKIDs6

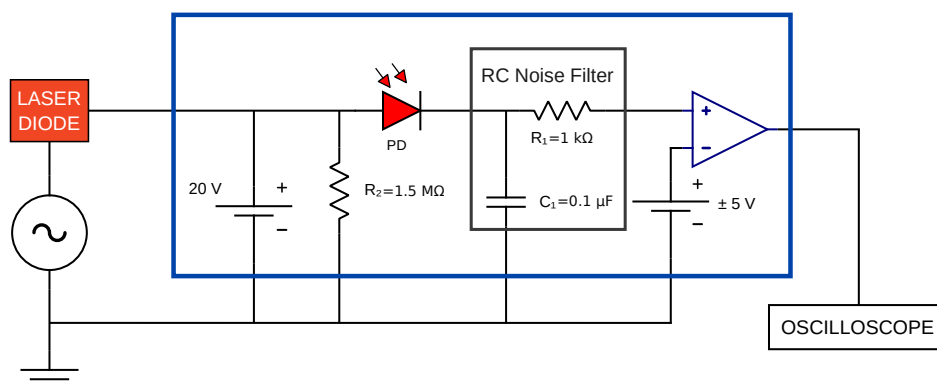


Figure 3: Schematics of the system used to characterize the diode. Starting from the left, a function generator powers the laser diode whose output is detected by a photodiode, coupled to an RC filter and an amplifier. The resulting signal is visualized with an oscilloscope.

employed. For the optical fiber segment inside the cryostat, precautions were taken to prevent degassing and vacuum leakage. The PVC and nylon layers of the optical fiber were removed, exposing its coating and cladding.

In this experiment, the MKIDs response is probed through the heterodyne readout scheme shown in fig. 4. The heterodyne technique allows measuring the phase and amplitude of S_{21} at the same time with an IQ mixer. This involves sending the same signal of frequency f through the circuit and the LO port of the mixer, while the transmitted signal is fed to the RF terminal. If the mixer is correctly calibrated, the resulting I and Q signals are proportional to the real and imaginary components of S_{21} .

The experimental procedure involves two distinct phases: detector characterization and photon detection. While the first one only required to use a VNA connected to the cryostat, the latter employed a custom circuit, shown in the scheme with solid lines. In both cases, to adapt the room-temperature thermal noise to the cryogenic environment, the probe signal is attenuated by -20 dB at the 4 K plate within the cryostat, and -20 dB at the mixing chamber, right before the MKIDs chip. A high-electron-mobility transistor (HEMT) is employed to amplify the signal from the detectors by $+36$ dB within the cryostat, allowing for the acquisition of a measurable signal.

The tool used to characterize the MKIDs is an HP-8753 VNA, which directly measured the S-matrix components. On the other hand, the photon detection scheme is more complex and involves multiple instruments to handle rapid changes in the resonant frequency. Additionally, the custom circuit allows for the simultaneous readout of two distinct MKIDs.

Two FSW-0010 synthesizers by QuickSyn are employed to generate the probe signals, one for each resonator. The two signals are then combined and transmitted via a single microwave line to the cryostat. The initial signal of $+15$ dB undergoes a

A postgraduate laboratory experiment to set up a single-photon detector using MKIDs⁷

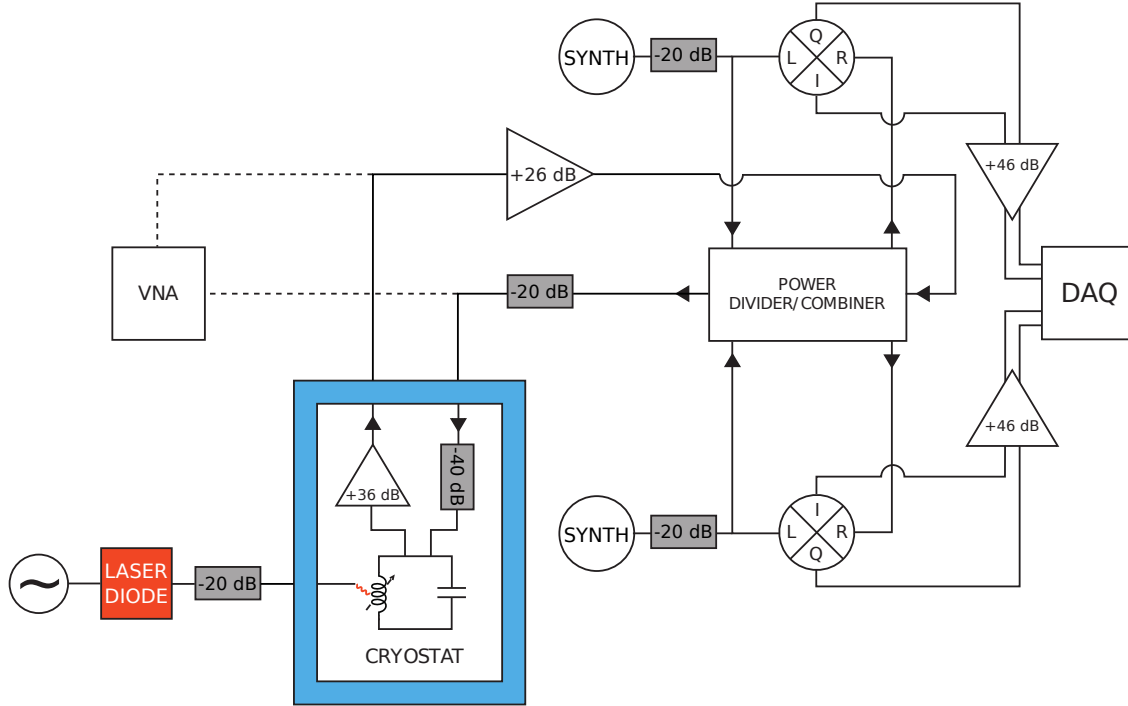


Figure 4: Circuit diagram for MKID characterization (dashed lines) and photon detection (solid lines). The latter allows for two resonators to be measured at the same time. The signal produced by a synthesizer is split and sent both to the LO port of an IQ mixer and to the cryostat. The output from the cryostat is then sent to the IQ mixer, this time as RF, resulting in I and Q signals which are acquired by the DAQ system.

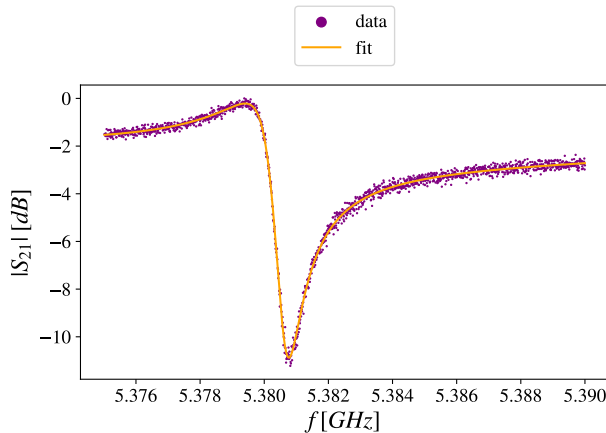
total attenuation of -80 dB, split between -40 dB within the cryostat and -40 dB from external attenuation. Additional amplification on top of that provided by the HEMT is given by a $+26$ dB RF amplifier placed outside of the cryostat. The channels are then split, and the signals are down-converted with two IQ mixers using the synthesizer's pulses as Local Oscillator. Down-conversion is necessary as the DAQ electronics used for the experiment (PXIe-5170R by National Instruments) operate in the MHz regime. Finally, the IQ components are further amplified by base-band amplifiers with a gain of $+46$ dB. Of the eight MKIDs present on the chip, only three have frequencies accessible with the employed VNA and heterodyne setup.

4. Experimental activities

4.1. MKIDs characterization

The first part of the experiment focuses on studying the MKIDs resonances, measuring resonant frequencies and quality factors in order to estimate the superconductor material gap Δ .

While keeping the minimum temperature achievable by the setup, in our case ~ 40



| Parameter | Value | Error |
|--------------|--------|-------|
| Q | 4050 | 20 |
| Q_i | 6440 | 40 |
| Q_c | 10600 | 140 |
| ϕ [rad] | 1.004 | 0.004 |
| f_0 [MHz] | 5380.6 | 0.1 |

Figure 5: Plot of one of the resonances, fitted with eq. (7). Relevant fitted parameters are shown in the table on the right.

mK, a raw estimate of the position of the resonances can be obtained using the VNA.

Once this has been done, it is possible to acquire their profiles as a function of the probe frequency and for different temperatures. This procedure is automated with two Python classes that allow remote control of the VNA and the cryostat's temperature. The resonances profiles are then fitted in order to extract the values of Q_i .

Both the amplitude and phase of S_{21} can be fitted using the module or the argument of eq. (7) respectively. This equation is a variant of eq. (2) that includes additional parameters to account for non-ideal responses. These consist in a phase ϕ_0 arising from mismatched impedances at the ports, which is responsible for the asymmetry of the resonance, and an overall complex constant a , which can be replaced by a low order polynomial to consider a non-flat background due to the entire readout line.

$$S_{21} = a \left(1 - \frac{Q}{Q_c} \frac{e^{j\phi_0}}{1 + 2jQ \frac{f-f_0}{f_0}} \right) \quad (7)$$

To estimate Δ , resonances were acquired at different temperatures ranging from 40 mK up to 300 mK in steps of 10 mK. Q and Q_c values were extracted from each fit, allowing for the determination of Q_i using eq. (3). The value of Δ was obtained using eq. (6), where α was determined from a simulation of the circuit with *Sonnet* [10].

As apparent in the trend of the curve in fig. 6, the fit function does not perfectly describe the data points, suggesting that the model is incomplete. This trend can be attributed to the Kondo effect [1, 9], which is caused by the interaction of magnetic impurities with conduction electrons. This effect is taken into account by adding a logarithmic term to the fit model:

$$\frac{1}{Q_i} = \frac{1}{Q(0)} + \frac{\alpha\sigma_1(T, \Delta)}{2\sigma_2(T, \Delta)} - b \ln \left(\frac{T}{T_K} \right) \quad (8)$$

where the two newly introduced free parameters are a multiplication coefficient b and the Kondo temperature T_K .

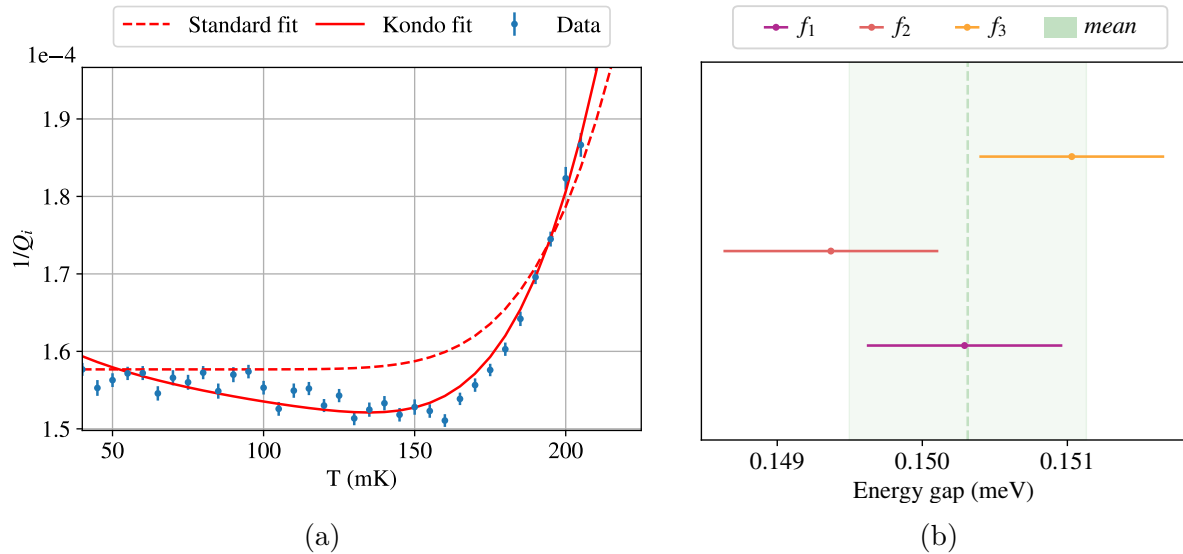


Figure 6: (a) Inverse of the internal quality factor as a function of temperature. The shift caused by the Kondo effect is clearly visible. (b) Fit results of the quality factors of three resonators and their weighted mean.

The results for Δ and T_c , shown in fig. 6, were obtained considering the weighted mean of the values from the three resonators:

$$\Delta = 0.150 \pm 0.001 \text{ meV}$$

$$T_c = 0.997 \pm 0.005 \text{ K}$$

4.2. Development of the data acquisition system

Another experimental activity that was carried out alongside the MKIDs characterization involved developing the data acquisition (DAQ) system for the custom photon detection setup.

As a first step, the FSW-0010 synthesizers were set to the MKIDs resonant frequencies, which fall within the 5 – 6 GHz range, in order to generate the probe signals.

The PXIe-5170R digitizer by National Instruments, which can sample frequencies up to 250 MSample/s/ch, was used for data acquisition. All four channels (I_1 , Q_1 , I_2 , Q_2) were used to exploit the multiplexing system. To determine the acquisition parameters such as the trigger, number of records to store, record length, and sample rate, a detailed signal analysis is required. Typical values used for data acquisition are 5×10^7 Hz for the sampling frequency, 6000 points for record length, and 1000 records per acquisition. The digitizer ADCs (Analog to Digital Converters) were configured to work within the range of ± 5 V and amplitude resolution of 14 bits.

One of the most critical aspects of data acquisition is the trigger, which should

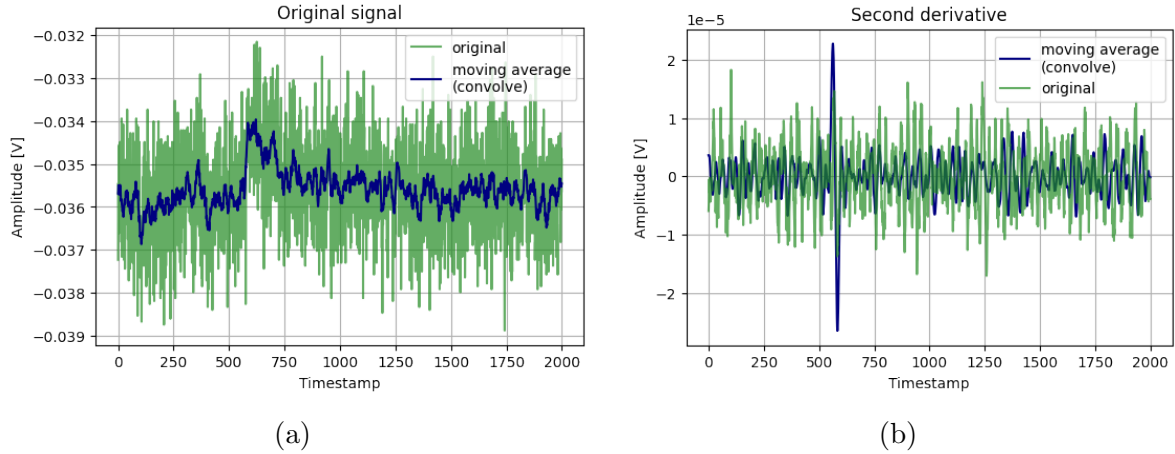


Figure 7: Smoothing techniques applied to raw signals. (a) The green line shows a raw signal profile, while the blue one shows the moving averaged signal. (b) The second derivative of both the original and processed signal with the application of the Savitzky-Golay filter.

efficiently select events while rejecting background noise or irrelevant processes. The most significant issue for the trigger used in this experiment was time jitter, which results in signals with the same amplitude triggering acquisition at different times. In order to correctly align the signals, which is crucial for the following data analysis, a moving average smoothing technique was first applied to reduce noise, as shown in fig. 7a.

The Savitzky-Golay filter [19] was then employed to smooth the second derivative of the signal. The filter works by fitting a polynomial function to a moving window of adjacent data points and substituting the central point of the window with the fitted value. It is then possible to compute the signal n -th derivative from the polynomial fit.

The second derivative of double exponential-like signals consists of a fast, bipolar signal with a baseline of zero. This spike can be used to establish the starting point of each signal (fig. 7b) and align them, reducing the time jitter.

4.3. IQ correction

The acquired raw data need to be corrected for the non-ideality of the experimental setup. This includes different procedures to calibrate warm electronics, namely IQ mixers and cable delays, and to standardize the MKIDs response.

The goal of this activity is to transform the raw acquired MKIDs resonances to correctly rotated and centered circles in the IQ plane. This correction will then be applied to each signal observed by the photon detectors. The following steps were employed:

Cable delay effect correction: both synthesizers and mixers are subject to a frequency-dependent offset. To address this issue, the RF port was disconnected,

and the acquisition was performed for different LO frequencies. The resulting profile was subtracted from the signal of interest.

IQ mixer calibration: Given sinusoidal LO and RF signals with similar frequencies, the response of an ideal IQ mixer consists of a circular pattern in the IQ plane. In a realistic IQ mixer, however, the phase between I and Q is not precisely 90° and the output is not balanced between the two ports. This results in observing an ellipse in the IQ plane. To calibrate each IQ mixer, two synthesizers at slightly different frequencies were connected to the LO and RF ports. The resulting signal was fitted with an ellipse, which was then mapped to a circle.

Background correction: even far from the MKIDs resonances, signals produced by the synthesizer arrive at the RF port with different amplitudes and phases. This leads to a frequency-dependent background which can be removed by fitting it with polynomial functions in a wide-frequency scan around the resonance. The fitted amplitude $A(\omega)$ and phase $\phi(\omega)$ are then used to correct the measured S_{21} for the on-resonance frequencies:

$$S_{21}(\omega) \rightarrow S_{21}(\omega) \frac{e^{-j\phi(\omega)}}{A(\omega)}$$

Center rotation : each resonance is fitted with a circle, which is then rotated around its center in order to align the resonance's gap with the I-axis.

Asymmetry rotation: the asymmetry in the shape of the resonance appears as a rotation of its circle in the IQ plane [13]. To correct this effect, a counter-rotation and a contraction must be applied:

$$S_{21} \rightarrow 1 - \cos(\theta)e^{j\theta}(1 - S_{21})$$

The overall effect of these corrections is shown in fig. 8.

4.4. Single photon analysis

At this point, the data used for photon detection should consist of a series of pulses recorded by the trigger and corrected as detailed in the previous section. For each pulse, amplitude and phase are obtained from the I and Q signal. The analysis focuses on the observed phase pulses, whose height can be linked to the photon energy.

A more precise energy estimator than the simple peak-to-peak height can be obtained by applying the Optimum Filter (OF) method [7]. The OF is able to achieve the best signal-to-noise ratio under the assumption that the signal is a linear combination of a mean signal and ergodic noise. This method allows the construction of a frequency filter that suppresses the frequencies where the noise contribution is more significant. There are various implementations of the filter, with the one used in this case being based on the Discrete Fourier Transform (DFT).

The OF takes in input some samples of noise and signals and outputs the frequency spectrum of the noise, the average pulse (average of the signals, fig. 9 (a)), and a transfer

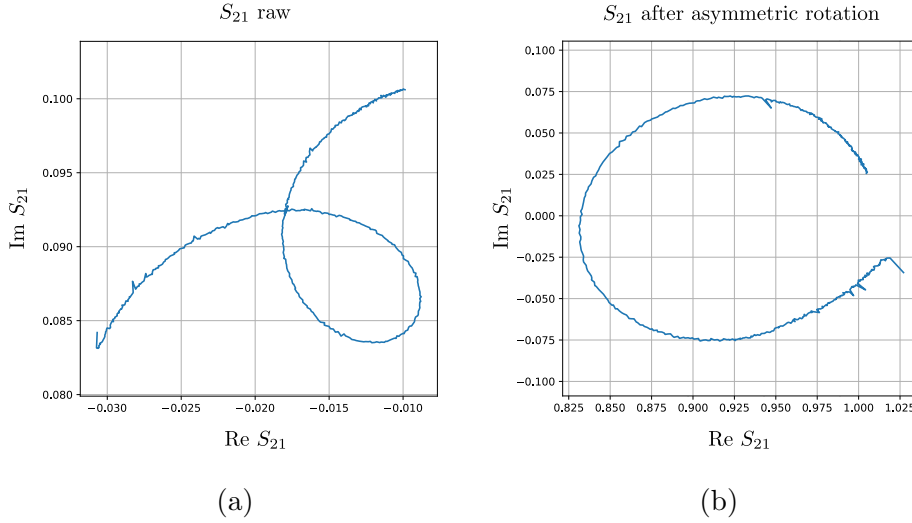


Figure 8: Correction of the resonance profile in the IQ plane. (a) Raw signal before applying IQ correction. (b) Corrected signal after applying IQ correction.

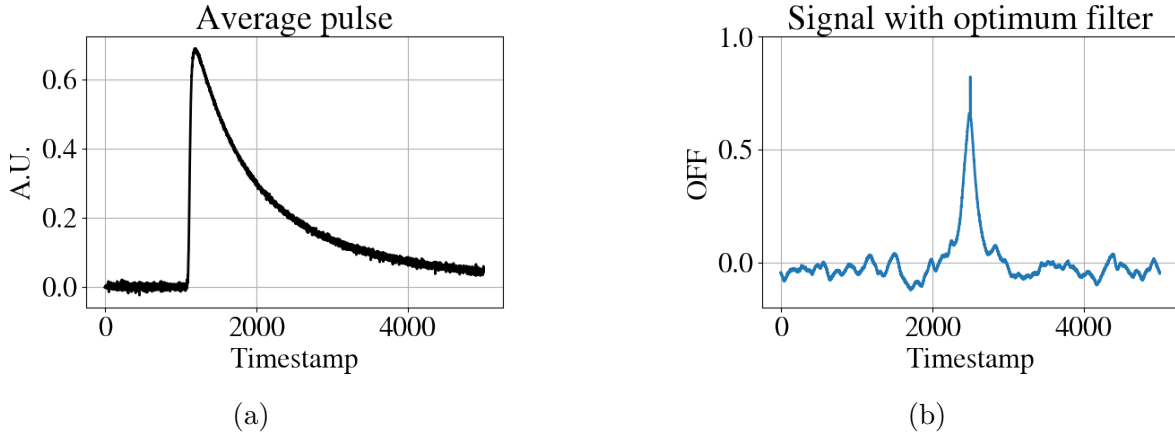


Figure 9: Example of Optimum Filter application. (a) Average pulse obtained from 2000 signals. (b) A signal filtered with the OF. The result is a cusp, the function with the best signal-to-noise ratio.

function that can be applied to the signals to reduce their noise component. The transfer function is then applied to the signals and the mean of the DFT of the filtered signal (OFF) is used as an estimator of the measured energy. An example of a signal after this step is shown in fig. 9 (b).

The expected energy spectrum is shown in fig. 10. When sending N photons to a detector, the number of photons that reach it follows a Poisson distribution with mean $\mu = N$. Assuming a Gaussian energy spread due to the finite detector's resolution, the observed spectrum is given by a sum of Gaussians weighted with a Poissonian distribution.

The expected spectrum can be used as a fit function for the observed data, which

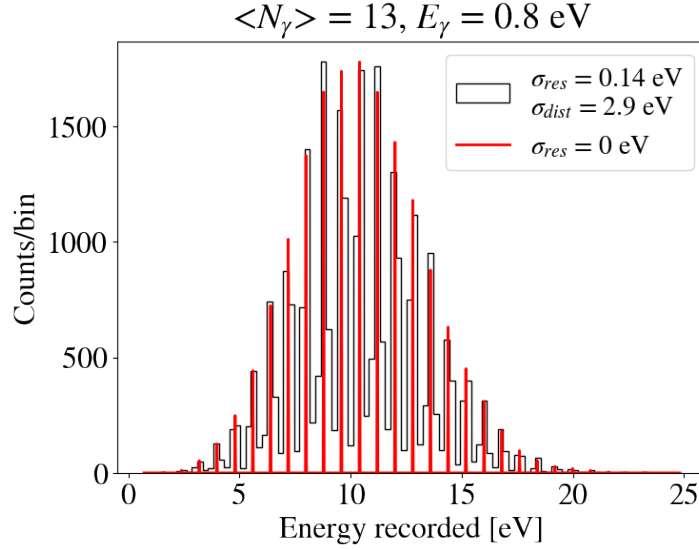


Figure 10: Simulation of the expected distribution of the amplitudes in the ideal case (red) with an infinite detector resolution and in a real case (black) with a finite resolution good enough to differentiate among the different peaks. σ_{res} is the detector resolution and σ_{dist} is the standard deviation of all the samples. In both cases, different peaks are visible and distinguishable.

are binned for different values of the OFF:

$$\text{model}(OFF, \sigma, \mu, A, \text{shift}, E_\gamma) = A \sum_{n=0}^{N_{max}} P(n; \mu) \cdot G(\text{OFF}; nE_\gamma + \text{shift}; \sigma) \quad (9)$$

where A is a normalization factor, N_{max} is a fixed maximum number of considered photons, $shift$ is a global shift of the fit function from zero, G is the Gaussian distribution, P is the Poisson distribution and E_γ is the conversion from A.U. to eV that can be obtained knowing the energy of one IR photon, i.e. 0.8 eV.

The measured distribution is shown in fig. 11. The peaks due to different photon numbers cannot be separated, likely due to the detector resolution being much larger than the photons energy.

The average number of photons can still be estimated with the fit. Due to the large number of parameters, it can be difficult to make the fit converge and more than one combination of parameters can give good χ^2 values. To avoid that, some parameters can be constrained. For example, σ is set to the detector's resolution, which is calculated as the Root Mean Squared (RMS) of the noise signals (after the OF) since it is the dominant component. All constraints are shown in the table in fig. 11.

The fit is conducted with `iminuit` [5], which is a Python implementation of the `Minuit2` C++ library [11]. The result of the fit, with a $\chi^2/\text{dof} = 1.2$, is shown in fig. 11. The best estimate for the average number of photons is 12 ± 2 .

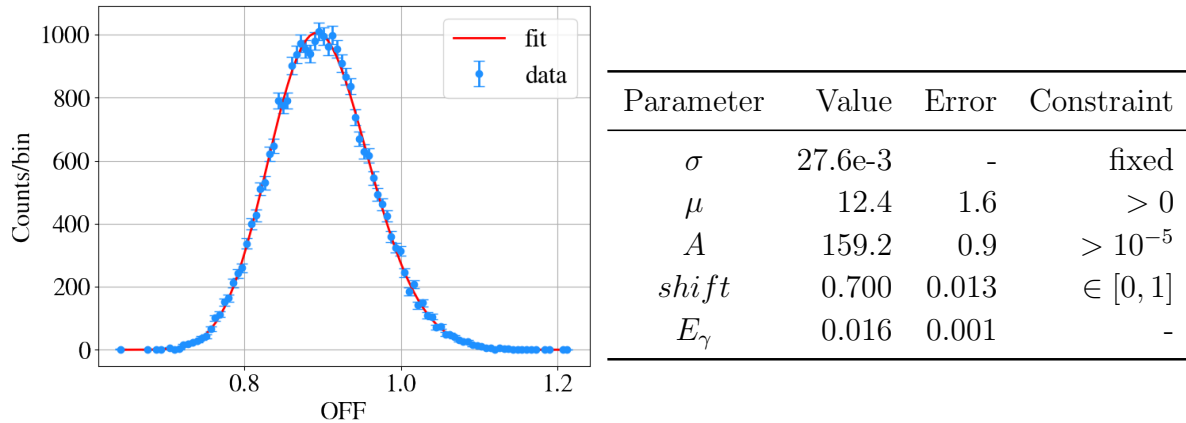


Figure 11: Histogram of the amplitudes computed with the OF. Data points are in blue, with error bars obtained assuming Poisson fluctuations in each bin, and the fit function is in red. The table on the right shows the best parameters found with the fit, with $\chi^2/\text{dof} = 1.2$. The last column shows the parameters' constraints.

5. Conclusions

This paper presented a laboratory experiment designed for postgraduate students in the field of quantum technologies, which aims to detect single photons in the far infrared range using Microwave Kinetic Inductance Detectors (MKID). The experiment involves characterizing the resonators and developing a data acquisition system to acquire the signals, concluding with the data analysis of the measurements using the characterized MKIDs.

The experience was first realized at the Università degli Studi di Milano-Bicocca in 2022 and the students reported an average number of observed photons of 12 ± 2 , even if the peaks due to different numbers of photons could not be resolved. Improvements in the experimental setup and the fabrication process of the MKIDs could enhance the resolution, allowing the distinction of different numbers of interacting photons as separate peaks in the energy spectrum.

Acknowledgments

A special thanks goes to our laboratory supervisors for the opportunity and their guidance in our experimental activities.

Disclaimer

Mention of commercial products is for information only and does not imply recommendation or endorsement.

References

- [1] A. A. Abrikosov. “Electron scattering on magnetic impurities in metals and anomalous resistivity effects”. In: *Physics Physique Fizika* (Sept. 1965). DOI: [10.1103/PhysicsPhysiqueFizika.2.5](https://doi.org/10.1103/PhysicsPhysiqueFizika.2.5).
- [2] J. Bardeen, L. N. Cooper, and J. R. Schrieffer. “Theory of Superconductivity”. In: *Phys. Rev.* 108 (5 Dec. 1957), pp. 1175–1204. DOI: [10.1103/PhysRev.108.1175](https://doi.org/10.1103/PhysRev.108.1175).
- [3] N. E. Booth and D. J. Goldie. “Superconducting particle detectors”. In: *Superconductor Science and Technology* 9.7 (July 1996), pp. 493–516. DOI: [10.1088/0953-2048/9/7/001](https://doi.org/10.1088/0953-2048/9/7/001).
- [4] P. K. Day et al. “A broadband superconducting detector suitable for use in large arrays”. In: *Nature* 425.6960 (Oct. 2003), pp. 817–821. ISSN: 1476-4687. DOI: [10.1038/nature02037](https://doi.org/10.1038/nature02037).
- [5] Hans Dembinski and Piti Ongmongkolkul et al. “scikit-hep/iminuit”. In: (Dec. 2020). DOI: [10.5281/zenodo.3949207](https://doi.org/10.5281/zenodo.3949207).
- [6] J. Gao. “The Physics of Superconducting Microwave Resonators”. PhD. California Institute of Technology, 2008. DOI: [10.7907/RATO-VM75](https://doi.org/10.7907/RATO-VM75).
- [7] E. Gatti and P. F. Manfredi. “Processing the signals from solid-state detectors in elementary-particle physics”. In: *La Rivista del Nuovo Cimento (1978-1999)* 9.1 (Jan. 1, 1986), pp. 1–146. ISSN: 1826-9850. DOI: [10.1007/BF02822156](https://doi.org/10.1007/BF02822156).
- [8] M. J. Hewitt et al. “Infrared readout electronics: a historical perspective”. In: SPIE, June 23, 1994. DOI: [10.1117/12.178474](https://doi.org/10.1117/12.178474).
- [9] A. C. Hewson and J. Kondo. “Kondo effect”. In: *Scholarpedia* (Mar. 11, 2009). DOI: [10.4249/scholarpedia.7529](https://doi.org/10.4249/scholarpedia.7529).
- [10] Sonnet Software Inc. *Getting Started*. 2013.
- [11] F and James. “MINUIT: Function Minimization and Error Analysis Reference Manual”. In: (1998). CERN Program Library Long Writeups. URL: <https://cds.cern.ch/record/2296388>.
- [12] Anush Kapoor, Prashant Kumar Varshney, and M. Jaleel Akhtar. “Interdigital capacitor loaded electric-LC resonator for dielectric characterization”. In: *Microwave and Optical Technology Letters* 62 (9 Sept. 2020), pp. 2835–2840. ISSN: 10982760. DOI: [10.1002/MOP.32391](https://doi.org/10.1002/MOP.32391).
- [13] M. S. Khalil et al. “An analysis method for asymmetric resonator transmission applied to superconducting devices”. In: *Journal of Applied Physics* 111.5 (Mar. 8, 2012). Publisher: American Institute of PhysicsAIP, p. 054510. ISSN: 0021-8979. DOI: [10.1063/1.3692073](https://doi.org/10.1063/1.3692073). URL: <https://aip.scitation.org/doi/abs/10.1063/1.3692073> (visited on 03/09/2023).
- [14] Henry G. Leduc et al. “Titanium nitride films for ultrasensitive microresonator detectors”. In: *Applied Physics Letters* 97.10 (2010), p. 102509. DOI: [10.1063/1.3480420](https://doi.org/10.1063/1.3480420).

- [15] D. C. Mattis and J. Bardeen. “Theory of the Anomalous Skin Effect in Normal and Superconducting Metals”. In: *Phys. Rev.* 111 (2 July 1958), pp. 412–417. DOI: [10.1103/PhysRev.111.412](https://doi.org/10.1103/PhysRev.111.412).
- [16] R. Mezzena et al. “Development of Microwave Kinetic Inductance Detectors for IR Single-Photon Counting”. In: *Journal of Low Temperature Physics* (Apr. 2020). DOI: [10.1007/s10909-019-02251-1](https://doi.org/10.1007/s10909-019-02251-1).
- [17] D. V. Morozov, A. Casaburi, and R. H. Hadfield. “Superconducting photon detectors”. In: *Contemporary Physics* 62 (Apr. 3, 2021), pp. 69–91. ISSN: 0010-7514. DOI: [10.1080/00107514.2022.2043596](https://doi.org/10.1080/00107514.2022.2043596).
- [18] David Pappas et al. “Two Level System Loss in Superconducting Microwave Resonators”. en. In: 21. *IEEE Transactions on Applied Superconductivity*, Washington, DC, Jan. 2011. DOI: <https://doi.org/10.1109/TASC.2010.2097578>.
- [19] A. Savitzky and M. J. E. Golay. “Smoothing and Differentiation of Data by Simplified Least Squares Procedures.” In: *Analytical Chemistry* 36.8 (July 1, 1964), pp. 1627–1639. DOI: [10.1021/ac60214a047](https://doi.org/10.1021/ac60214a047).
- [20] James A. Schlaerth. “Microwave kinetic inductance detector camera development for millimeter-wave astrophysics”. PhD thesis. University of Colorado, Boulder, Jan. 2010.
- [21] G. Ulbricht, M. De Lucia, and E. Baldwin. “Applications for Microwave Kinetic Induction Detectors in Advanced Instrumentation”. In: *Applied Sciences* 11.6 (Mar. 17, 2021), p. 2671. ISSN: 2076-3417. DOI: [10.3390/app11062671](https://doi.org/10.3390/app11062671).